

Visibility graph analysis of intraspinal pressure signal predicts functional outcome in spinal cord injured patients

Suliang Chen PhD¹, Mathew J. Gallagher MB ChB¹, Florence Hogg MB ChB¹, Marios C. Papadopoulos MD^{1*}, Samira Saadoun PhD^{1*}

¹Academic Neurosurgery Unit, St. George's, University of London, London, U.K.

*Co-senior authors

Correspondence: Dr. S. Saadoun, ssaadoun@sgul.ac.uk

Running title: Intraspinal pressure after spinal cord injury

Table of contents title: Visibility graph analysis of intraspinal pressure after spinal cord injury

Abbreviations: AIS, American spinal injuries association Impairment Scale; CPP, cerebral perfusion pressure; ICP, intracranial pressure; ICU, intensive care unit; ISCoPE, Injured Spinal Cord Pressure Evaluation study; MAP, mean arterial pressure; SCPP, spinal cord perfusion pressure, sPRx, spinal cord vascular pressure reactivity index; σ , small-world coefficient; TBI, traumatic brain injury; TSCI, traumatic spinal cord injury

Suliang Chen PhD, Postdoctoral Research fellow, Academic Neurosurgery Unit, Molecular and Clinical Sciences Institute, St. George's, University of London, London SW17 0RE, United Kingdom. Tel. +44(0)2087254179; Email. schen@sgul.ac.uk

Mathew J. Gallagher MB ChB, Doctoral Research student, Academic Neurosurgery Unit, Molecular and Clinical Sciences Institute, St. George's, University of London, London SW17, United Kingdom. Tel. +44(0)2087254179; Email. magallag@sgul.ac.uk

Florence Hogg MB ChB, Doctoral Research student, Academic Neurosurgery Unit, Molecular and Clinical Sciences Institute, St. George's, University of London, London SW17 0RE, United Kingdom. Tel. +44(0)2087254179; Email. fhogg@sgul.ac.uk

Marios C. Papadopoulos MD, Professor of Neurosurgery, Academic Neurosurgery Unit, Molecular and Clinical Sciences Institute, St. George's, University of London, London SW17 0RE, United Kingdom. Tel. +44(0)2087254179; Email. mpapadop@sgul.ac.uk

Samira Saadoun PhD, Senior Lecturer in Neuroscience Academic Neurosurgery Unit, Molecular and Clinical Sciences Institute, St. George's, University of London, London SW17 0RE, United Kingdom. Tel. +44(0)2087254179; Email. ssaadoun@sgul.ac.uk

Abstract

To guide management of patients with acute spinal cord injuries, we developed intraspinal pressure monitoring from the injury site. Here, we examine the complex fluctuations in the intraspinal pressure signal using network theory. We analyzed 7,097 hours of intraspinal pressure data from 58 patients with severe cord injuries. Intraspinal pressure signals were split into hourly windows. Each window was mapped into a visibility graph as follows: Vertical bars were drawn at 0.1 Hz representing signal amplitudes. Each bar produced a node, thus totalling 360 nodes per graph. Two nodes were linked with an edge if the straight line through the nodes did not intersect a bar. We computed several topological metrics for each graph including diameter, modularity, eccentricity and small-worldness. Patients were followed up for 20 months on average. Our data show that the topological structure of intraspinal pressure visibility graphs is highly sensitive to pathological events at the injury site including cord compression (high intraspinal pressure), ischemia (low spinal cord perfusion pressure) and deranged autoregulation (high spinal pressure reactivity index). These pathological changes correlate with long graph diameter, high modularity, high eccentricity and reduced small-worldness. In a multivariate logistic regression model, age, neurological status on admission and average node eccentricity were independent predictors of neurological improvement. We conclude that analysis of intraspinal pressure fluctuations after spinal cord injury as graphs, rather than time series, captures clinically important information. Our novel technique may be applied to other signals recorded from injured CNS e.g intracranial pressure, tissue metabolite and oxygen levels.

Manuscript keywords: Intensive Care Unit, Intraspinal pressure, Monitoring, Network theory, Spinal cord injury

Introduction

Traumatic spinal cord injury (TSCI) is a devastating condition with generally poor outlook¹,². Most patients are young males with complete injuries who remain paralyzed without control of bladder, bowel or sexual function. There is no treatment proven to improve outcome after acute, severe TSCI³ and, consequently, current medical and surgical management practices are variable⁴. Following the primary injury, further cord damage may occur e.g. from ongoing cord compression, low blood pressure⁵, peripheral infections⁶ and fever⁷.

To prevent such secondary cord damage, we introduced monitoring from the injury site in patients in the intensive care unit (ICU)^{1,8,9}. We monitor intraspinal pressure (ISP), spinal cord perfusion pressure (SCPP) and the vascular pressure reactivity (sPRx), which is used to compute the optimum SCPP¹⁰. These monitoring techniques are safe¹¹ and are analogous to monitoring intracranial pressure (ICP) and cerebral perfusion pressure (CPP) after traumatic brain injury (TBI). Several lines of evidence suggest that ISP and SCPP are clinically important physiological parameters: first, higher SCPP correlates with better injury site metabolism (higher glucose, lower lactate-to-pyruvate ratio, lower glutamate, lower glycerol) determined by microdialysis¹². Second, intervention to increase SCPP in TSCI patients improves neurological status in some patients¹. Third, lower mean ISP and higher mean SCPP correlate with improved long-term neurological outcome¹³. Fourth, intervening to increase SCPP increases the amplitude of motor evoked responses monitored from below the injury site in some patients¹.

The ISP signal (and its brain equivalent, the ICP) is a complex time series; therefore, conventional analysis e.g. computing mean ISP amplitude, loses biologically important information hidden within the various complex patterns of signal fluctuations. To access such

hidden information, we analyzed the ISP signals from a different perspective. We first map each hourly ISP time series into a visibility graph¹⁴. We then determine the topological structure of these graphs using analytical tools developed in complex network theory e.g. diameter, modularity, eccentricity and small-worldness¹⁵. Our data show that the topological characteristics of ISP graphs are highly sensitive to adverse events at the injury site such as cord compression (increased ISP), hypoperfusion (reduced SCPP) and impaired vascular pressure reactivity (increased sPRx). Remarkably, these topological metrics correlate with neurological outcome.

Materials and Methods

Approvals. Patients were part of the Injured Spinal Cord Pressure Evaluation (ISCoPE) study (<https://clinicaltrials.gov>, NCT02721615). Approvals were obtained from the St George's, University of London Joint Research Office and the National Research Ethics Service London–St Giles Committee. Informed consent was obtained from all participants included in the study.

Patient recruitment. All patients were treated at the Department of Neurosurgery and the Neuro-ICU at St. George's Hospital in London. ISCoPE inclusion criteria are: 1. Severe TSCI defined as American spinal injuries association Impairment Scale (AIS) grades A–C; 2. Age 18–70 years; 3. Timing between TSCI and surgery ≤ 72 hours. Exclusion criteria are: 1. Unable to consent; 2. Major co-morbidities; 3 Penetrating TSCI. This is a consecutive series of ISCoPE patients from 2010–2017.

Insertion of intraspinal pressure probe. After bony realignment and posterior fixation, the ISP probe (Codman Microsensor Transducer®, Depuy Synthes, Leeds, UK) was placed intraoperatively under the dura on the spinal cord surface at the site of maximal cord swelling as determined from the MRI. The probe monitors pressure, which is generated by the swollen injured cord compressed against the dura. These ISP recordings differ from corresponding values obtained from proximal or distal cord or extradurally. Details are given elsewhere ^{1, 8, 11-13, 16, 17}.

Intraspinal pressure, spinal cord perfusion pressure. The ISP probe was connected to a Codman ICP box linked via a ML221 amplifier to a PowerLab running LabChart v.7.3.5 (AD Instruments, Oxford, UK). Arterial blood pressure was recorded from a radial artery catheter kept at heart level and connected to a Philips Intellivue MX800 bedside monitoring system (Philips, Guildford, UK) in turn connected to the PowerLab system. ISP and arterial blood pressure signals were sampled at 1 kHz for up to 7 days. LabChart was used to analyse the signals and compute SCPP as mean arterial pressure (MAP) minus ISP. Spinal pressure reactivity index (sPRx) was computed as the running correlation coefficient over 5 minutes between MAP and ISP. Details are given elsewhere ^{1, 8, 11-13, 16, 17}.

Patient assessments. Neurological examinations to record the AIS grade were done by neurosurgical research fellows who are experienced neurosurgical residents trained according to the International Standards for Neurological Classification of Spinal Cord Injury. Patients were examined on admission, prior to discharge to the spinal rehabilitation centre and during outpatient appointments. A CT and MRI of the whole spine were done on admission, another CT within 48 hours of surgery, another MRI within two weeks of surgery and another MRI at 6 – 12 months after surgery.

Converting intraspinal pressure signals into graphs. The ISP time series was re-sampled at 0.1 Hz and split into non-overlapping hourly windows. The natural visibility algorithm proposed by Lacasa et al. ¹⁴ was programmed into MATLAB (<https://uk.mathworks.com>) and applied to each hourly ISP signal to identify nodes and links and obtain the adjacency matrix, which shows if points (nodes) are visualized by other nodes. The algorithm maps each 0.1 Hz ISP value onto a node, which is connected to any node that has a visibility link. For details see Supplement.

Graph metrics. We characterized the following topological metrics for each graph: *Graph diameter* is the shortest path between the two most distant nodes ¹⁵. *Graph modularity* measures how a graph is structured and identifies communities/clusters ¹⁸. *Graph eccentricity* captures how important nodes are in a graph ¹⁵. We computed average E. *Clustering coefficient* indicates the extent to which neighbors of a node are neighbors of each other. *Average path length* shows, on average, the number of steps it takes to get from one node to another. *Small-worldness* is quantified by the coefficient σ . If $\sigma > 1$, then the graph is small-world, i.e. it is characterized by high clustering coefficient and short average path length ¹⁹. Each measure gives a single value per hourly ISP graph that can be plotted against corresponding hourly ISP, SCPP and sPRx values. For details see Supplement.

Graph visualization. The adjacency matrix was analyzed using the Girvan-Newman algorithm ¹⁸ to detect embedded groups/clusters of nodes within the graph. To display the graphs, node data (node ID, degrees) and edge data (source nodes, target nodes, weights) were imported into GEPHI (v.0.9.2, <https://gephi.org>) within the MATLAB environment. The FORCEATLAS2 layout algorithm within GEPHI was used to disperse groups of nodes

and give space around larger nodes. We checked “prevent overlap” and set “scaling” to 50 in the parameter settings. The function was kept running until the network was mostly stabilized. Nodes and edges were then coloured to display clusters, centrality and quality features of the graph.

Simulated signals. We investigated the effect of different types of signal fluctuations on graph topology, by considering the effect of the following modifications on a sinusoidal signal: no modification, narrow trough, narrow peak, transiently elevated baseline, wide peak, and wide peak with smaller peaks on top. We chose these modifications based on our observations of many ISP signals, aiming to model clinically important events: For example, in our earlier work we showed that a regular ISP signal has low complexity and is pathological²⁰. High ISP, as occurs after a severe TSCI, often has transient troughs. A normal ISP signal, as occurs with less severe TSCI, has transient narrow peaks and its baseline fluctuates due to respiration and autoregulatory response to changes in MAP. After a severe TSCI, there are often prolonged elevations in ISP.

Statistics. Data are shown as mean +/- standard error. We computed Pearson correlation coefficients. Data are shown as mean +/- standard error (sem). Statistical significance was taken at $P < 0.05$. Logistic regression analysis was done using XLStat Biomed v.2018.1 using the logit model. For multivariate logistic regression, we chose the best model with minimum of 1 and maximum of 8 variables to maximize the likelihood ratio.

Results

Patient details. During the study period, 61 consecutive patients met the inclusion/exclusion criteria and were asked to enter the study: 59 patients accepted and 2 patients refused. We thus recruited 59 TSCI patients. In one patient, the ISP probe became dislodged and, therefore, data from 58 patients are analyzed. Patients were generally young (81.0 % less than 60 years old) and mostly male (79.3 %). Most patients (69.0 %) had complete TSCI (i.e. AIS grade A) on admission. About half of them had cervical injuries (51.7 %) and half (48.3 %) thoracic/lumbar injuries. All patients underwent posterior surgical approaches, but 14.2 % also had anterior surgery. On average, ISP monitoring continued for 5 – 6 days after surgery in ICU. Mean follow-up was 20 months in patients who improved AIS grade(s) and those who did not. Patient details are summarized in Table 1.

Complications. In this patient cohort, we recorded the following complications, likely related to ISP monitoring: pseudomeningocele (15/58, 25.9 %), CSF leak (8/58, 13.8 %), meningitis (0/58, 0.0 %), wound infection (0/58, 0.0 %), probe-associated hematoma or cord damage (0/58, 0.0 %) and worse AIS grade (0/58, 0.0 %). Pseudomeningocele was detected on the first postoperative MRI done at 1 – 2 weeks after surgery and resolved on MRI done at 6 – 12 months. CSF leak through probe skin exit sites or through the wound during monitoring stopped by placing extra skin sutures. There was no need to re-operate on any patient as a result of ISP monitoring.

Visibility graphs. Fig. 1A shows examples of ISP and MAP signals obtained from the injury site of a patient. The signals were imported into ICM+ to compute SCPP and sPRx (Fig. 1B). ISP data were transformed into visibility graphs as summarized in Fig. 1C. ISP time series were first divided into non-overlapping hourly windows. For each window, vertical bars were drawn at regular intervals representing ISP amplitude such that each bar corresponds to a

node in the graph. Two nodes were linked with an edge if the straight line linking the nodes did not intersect a bar. The adjacency matrix A_{ij} was then constructed with entries '1' if two nodes are linked or '0' if unlinked. Though we computed many topological metrics of ISP graphs, here we focus on D , Q , E and σ .

Graph diameter. Diameter is the geodesic path between the two nodes that are furthest apart. Figs. 2A-B show examples of two hourly ISP signals and their respective graphs, one with long and one with short diameter. We found strong positive correlation between ISP and graph diameter as well as between sPRx and graph diameter, but strong negative correlation between SCPP and graph diameter (Fig. 2C). Thus, cord compression, ischemia and loss of autoregulation are associated with increased graph diameter. Fig. 2D shows the effect of various ISP fluctuations on graph diameter. A sinusoidal signal has long diameter. Introducing a narrow trough only slightly shortens the diameter, but a narrow peak or transiently elevated baseline greatly reduces the diameter by providing bridging nodes. A wide peak with or without smaller peaks on top has little influence on the diameter. Thus, irregular signals with transient peaks or transient baseline elevations have short diameter, whereas regular signals or signals with prolonged elevations have longer diameter.

Graph modularity. The nodes within a graph may form cliques, such that nodes within a clique are strongly linked, but cliques only weakly link with each other. Modularity measures how well cliques link between them and is high if the cliques poorly inter-link. Figs. 3A-B show examples of two ISP hourly signals and their respective graphs, one with high and one with low modularity. There was strong positive correlation between ISP and graph modularity, strong negative correlation between SCPP and graph modularity, but no correlation between sPRx and graph modularity (Fig. 4C). These data suggest that cord

compression and ischemia, but not loss of autoregulation, are associated with increased graph Q. Fig. 3D uses model signals to explain how different signal fluctuations influence modularity. A sinusoidal signal with or without a narrow trough or peak, with or without flat baseline has zero modularity. A tall, wide peak increases modularity by splitting the graph into two poorly inter-linked modules. Peaks on top of the wide peak slightly increase the number of links between the modules thus slightly reducing modularity.

Graph eccentricity. To find eccentricity, we compute the geodesic path between node i and each other node and choose the longest of these paths. Thus, if the eccentricity of a node is high, then at least one other node lies far from it. Low eccentricity means that all other nodes are near. Averaging the eccentricity values of all the nodes yields the average eccentricity of the graph. Figs. 4A-B show examples of two ISP hourly signals and their respective graphs, one with high and one with low average eccentricity. We found strong positive correlation between ISP and average eccentricity as well as between sPRx and average eccentricity, but strong negative correlation between SCPP and average node eccentricity (Fig. 2C). These data suggest that cord compression, ischemia and loss of autoregulation are associated with increased graph average node eccentricity. Fig. 4D shows how fluctuation patterns in the ISP signal influence the eccentricity. A sinusoidal signal has generally high eccentricities. A narrow trough only slightly reduces average eccentricity, but a narrow peak or transiently elevated baseline greatly reduces average node eccentricity by providing bridging nodes. A wide peak increases average eccentricity, but smaller peaks on top of the wide peak only modestly influence eccentricity. Thus, signals with transient peaks or transient baseline elevations have low eccentricities, but regular signals or prolonged elevations increase eccentricity.

Graph small-worldness. A small-world graph is characterized by high clustering coefficient and short average path length. This means that most nodes are not directly linked, but any nodes directly linked to a node are likely to be linked to each other. Also, most nodes can be reached from any other node by a small number steps. Because small-world graphs have special properties and are ubiquitous in nature ¹⁹, we investigated whether the ISP signals produce small-world graphs. Figs. 5A-B show examples of two ISP hourly signals and their respective graphs, one with high and one with low σ . We found strong negative correlation between ISP and σ as well as between sPRx and σ , but strong positive correlation between SCPP and σ (Fig. 5C). These data suggest that cord compression, ischemia and loss of autoregulation are associated with reduced σ of ISP graphs. Fig. 5D shows how fluctuation patterns in the ISP signal may influence the ratio of clustering coefficient to average path length, a measure of small-worldness. A sinusoidal signal has low σ . A narrow trough only slightly increases clustering coefficient and reduces average path length thus slightly increasing σ . A narrow peak or transiently elevated baseline slightly increase clustering coefficient, but greatly reduce average path length thus greatly increasing σ . A wide peak reduces clustering coefficient and increases average path length thus reducing σ . Small peaks on top of a wide peak do not affect clustering coefficient and slightly reduce average path length thus only modestly influencing σ . Overall, signals with transient peaks or transient baseline elevations have high σ , but regular signals or signals with prolonged elevations have low σ .

Patient outcome. At follow-up, 65.5 % (38/58) patients did not improve, 17.2 % (10/58) improved by one AIS grade, 15.5 % (9/58) by two or more grades and 1.8 % (1/58) were lost to follow-up. Fig. 6 shows that shorter graph diameter, smaller average node eccentricity, lower modularity and higher σ correlate with AIS grade improvement. In univariate analysis,

the following variables significantly correlated with AIS grade improvement: Higher AIS grade on admission, younger patient age, lower ISP (average of entire signal), higher SCPP (average of entire signal), shorter graph diameter, lower modularity, lower average node eccentricity, higher σ . For each patient, we averaged graph diameter, modularity and mean node eccentricity over all ISP graphs. In multivariate analysis, AIS grade on admission, SCPP and graph average node eccentricity remained independent prognostic factors. The odds ratios indicate the following: A patient with one higher AIS grade on admission than another, has 4.2× better chance of AIS grade conversion at follow-up. For every 1 mmHg increase in average SCPP, there is 10 % higher chance of AIS grade conversion at follow-up. For every 1 unit increase average node eccentricity, there is 90 % lower chance of AIS grade conversion at follow-up. The results of univariate and multivariate logistic regression analysis are summarized in Table 2. The corresponding Receiver Operated Characteristic (ROC) curve for the multivariate model had Area Under Curve (AUC) value of 0.845, indicating a good classifier. A Leave-One-Out cross validation (LOO-CV) yielded a classification accuracy of 73.65 %. Details are in the Supplement.

Discussion

We showed that ISP signals can be converted into graphs using the visibility algorithm. The graphs can then be analyzed using the powerful tools of complex network theory to quantify their topological structures including size, presence of clusters, connections between clusters, accessibility of nodes from other nodes, APL, and small-world properties. Our key finding is that these graphs inherit in their topologies fundamental information from the original ISP time series. The topological structures of ISP graphs are, therefore, highly sensitive to the pathological changes that occur at the injury site e.g. cord compression (high ISP), ischemia

(low SCPP) and impaired autoregulation (high sPRx). The visibility algorithm thus allows the complex dynamics of the ISP signal to be analyzed from a novel angle.

What are the advantages of analyzing ISP as graphs instead of time series? Time series are used to compare amplitudes (e.g. mean, trend, variability) that have clinical meaning¹. For example, higher mean ISP means more severe cord compression. If ISP is decreasing, then cord compression is improving. High ISP variability may indicate mechanical spinal instability causing fluctuating cord compression. Time series are also used to identify correlations with biological meaning e.g. higher ISP correlates with worse neurological outcome¹³, when ISP increases then sPRx increases (impaired autoregulation)¹,⁸ and tissue lactate to pyruvate ratio also increases (increased tissue ischemia)¹². Unlike time series, ISP graph topology is not affected by ISP amplitude¹⁴; a sinusoidal signal produces identical visibility graphs regardless of whether it fluctuates between +5 and +10 or between +30 and +35. Graph topology is, however, sensitive to patterns of fluctuations that may have little effect on amplitude; a narrow peak or transient rise in ISP baseline provides bridging nodes that reduce graph D and average E and increase σ . In contrast, a periodic signal has long graph D, high E and low σ . Q increases with wide peaks in the signal, but, compared with a sinusoidal signal, baseline signal fluctuations do not reduce Q. Such fluctuation patterns may have biological meaning. For example, a normal ISP or ICP signal has irregularities e.g. narrow peaks (straining, coughing) and a fluctuating baseline (from respiration or autoregulatory response to fluctuations in MAP)^{1,8}, which may reduce D, E and increase σ . With increased cord compression, ISP exhibits large, wide peaks that may increase D, E and Q as well as reducing σ . Loss of autoregulation would increase D and E as well as reducing σ without much effect on Q. Thus, the various graph metrics used here likely capture clinically important information that is difficult to appreciate from the original ISP signal. This may explain why these graph metrics correlate with patient outcome. The

multivariate logistic regression model, based on AIS grade on admission, SCPP and graph average node eccentricity has good predictive value evident by the high AUC value of the ROC curve and the high classification accuracy of LOO-CV. The prognostic power of the graph metrics requires additional validation in future studies using different sets of TSCI patients.

Unlike ISP monitoring for TSCI, ICP monitoring for severe TBI has been the standard of care in developed countries for many years^{21,22}. The early management of patients with TBI is focused on limiting secondary injury by reducing ICP below 25 mmHg and increasing CPP above 60 mmHg. Our group has developed analogous techniques for monitoring ISP and SCPP in patients with TSCI^{1,8,11}. Recently, the value of ICP monitoring in TBI has been questioned because of absence of Class I evidence that ICP-directed management improves outcome²³. Large observational studies^{24,25} and sophisticated analysis of ICP signals²⁶ indicate that ICP-directed treatments have the potential to improve outcome, provided that patient care is targeted to individualized optimal CPP values that vary widely between patients. The ISP monitoring field has a lot to learn from the pitfalls of ICP monitoring e.g. by avoiding universal treatment thresholds and individualizing management instead¹⁰. ISP monitoring is invasive, but the complications are not serious and include CSF leak through the probe skin exit site, pseudomeningocele and probe dislodgement¹¹. To date, we have used AIS grade conversion as the only outcome measure; in future studies, other outcome measures should also be used to make the findings more robust. In TBI patients, some neuro-ICUs monitor tissue oxygen and metabolism in addition to ICP and CPP^{27,28}. This is also possible in TSCI patients by using microdialysis to monitor injury site metabolism^{12,16}. Though monitoring many physiological and biochemical parameters from the injury site makes sense, the clinical value of multi-modality monitoring has been challenged, because of the lack of clinically relevant analysis techniques. Visualizing data as

networks, as described here, might make clinically relevant changes in the monitored parameters easier to appreciate.

Transformation of time series into graphs has only become possible recently¹⁴. There have been several attempts to apply this technique in medicine e.g. predict the onset of ventricular fibrillation by ECG²⁹, diagnose Alzheimer's disease³⁰ or analyze seizure patterns by EEG³¹, and outside medicine e.g. predict the magnitude of growth of stock prices using price time series³² or predict tourist demand for holiday resorts³³. These techniques could also be applied to ICP signals after TBI and other signals recorded from injured brain or spinal cord e.g. tissue oxygen or metabolite levels monitored by microdialysis. A sliding one-hour window updated every minute could be used to provide real-time information in ICU on ISP graph topology.

We showed that ISP graphs have small-world properties. There are many examples of small-world networks in nature including chemical reaction networks, healthy neuronal connections, social networks and networks of world airports³⁴. Small-worldness confers advantages to networks such as robustness to external insults, scale invariance as well as efficient storage, transmission and retrieval of information. Our data indicate that the small-worldness metric σ decreases with increasing cord compression, decreasing cord perfusion and more deranged cord autoregulation. Thus, as the secondary insults become more severe, ISP graphs become more disorganised with longer average path length and smaller clustering coefficient. These topological changes in the ISP graphs likely arise from disorganization in the various processes that give rise to the ISP signal e.g. cardiac and respiratory pulsations, intraspinal compliance, spinal cord blood flow, oxygenation and metabolism. Therefore, σ provides information about the state of the injury site from a novel perspective.

Since the original paper reporting the natural visibility algorithm, several variations have been published. Directed graphs could be used to incorporate temporal information in

the network e.g. if node i corresponds to a future time than node j , and are visible to each other, then there is connection from $i \rightarrow j$ but not $i \leftarrow j$ ³⁵. There is also a technique to map multivariate time series into multiplex graphs³⁶ that may enable analysis of multi-modality monitoring data from the injury site e.g. ISP, tissue oxygen and microdialysis. Such studies are beyond the scope of this paper. Our study has provided proof of principle that this novel research avenue is interesting to pursue when analysing and interpreting complex signals from injured brain or spinal cord.

Acknowledgements

We thank the neurosurgeons at St. George's, King's College and Royal Sussex County Hospitals for help with patient recruitment. We thank the anaesthetic, neurointensive care and operating theatre staff at St. George's for help with probe insertion and data collection.

Funding

This work was supported by the Wings for Life Spinal Cord Research Foundation, the Fletcher Fund, the Neurosciences Research Foundation and the London Deanery.

Author contributions statement

SC wrote software and analysed the data to produce all the networks and metric data. MG and FG collected and cleaned the raw data and patient demographics. MP performed the surgical procedures, looked after the patients and inserted the probes. MP and SS analyzed data, produced the figures and wrote the manuscript. SS supervised the project.

Author Disclosures

No competing financial interests exist.

References

1. Werndle, M.C., Saadoun, S., Phang, I., Czosnyka, M., Varsos, G.V., Czosnyka, Z.H., Smielewski, P., Jamous, A., Bell, B.A., Zoumprouli, A. and Papadopoulos, M.C. (2014). Monitoring of spinal cord perfusion pressure in acute spinal cord injury: initial findings of the injured spinal cord pressure evaluation study. *Crit Care Med* 42, 646-655.
2. Lee, B.B., Cripps, R.A., Fitzharris, M. and Wing, P.C. (2014). The global map for traumatic spinal cord injury epidemiology: update 2011, global incidence rate. *Spinal Cord* 52, 110-116.
3. van Middendorp, J.J., Goss, B., Urquhart, S., Atresh, S., Williams, R.P. and Schuetz, M. (2011). Diagnosis and prognosis of traumatic spinal cord injury. *Global Spine J* 1, 1-8.
4. Werndle, M.C., Zoumprouli, A., Sedgwick, P. and Papadopoulos, M.C. (2012). Variability in the treatment of acute spinal cord injury in the United Kingdom: results of a national survey. *J Neurotrauma* 29, 880-888.
5. Ahuja, C.S., Wilson, J.R., Nori, S., Kotter, M.R.N., Druschel, C., Curt, A. and Fehlings, M.G. (2017). Traumatic spinal cord injury. *Nat Rev Dis Primers* 3, 17018.
6. Failli, V., Kopp, M.A., Gericke, C., Martus, P., Klingbeil, S., Brommer, B., Laginha, I., Chen, Y., DeVivo, M.J., Dirnagl, U. and Schwab, J.M. (2012). Functional neurological recovery after spinal cord injury is impaired in patients with infections. *Brain* 135, 3238-3250.
7. Gallagher, M.J., Zoumprouli, A., Phang, I., Schwab, J.M., Kopp, M.A., Liebscher, T., Papadopoulos, M.C. and Saadoun, S. (2018). Markedly deranged injury site metabolism and impaired functional recovery in acute spinal cord injury patients with fever. *Crit Care Med*, In press.

8. Varsos, G.V., Werndle, M.C., Czosnyka, Z.H., Smielewski, P., Koliass, A.G., Phang, I., Saadoun, S., Bell, B.A., Zoumprouli, A., Papadopoulos, M.C. and Czosnyka, M. (2015). Intraspinal pressure and spinal cord perfusion pressure after spinal cord injury: an observational study. *J Neurosurg Spine* 23, 763-771.
9. Saadoun, S. and Papadopoulos, M.C. (2016). Spinal cord injury: is monitoring from the injury site the future? *Crit Care* 20, 308.
10. Chen, S., Smielewski, P., Czosnyka, M., Papadopoulos, M.C. and Saadoun, S. (2017). Continuous Monitoring and Visualization of Optimum Spinal Cord Perfusion Pressure in Patients with Acute Cord Injury. *J Neurotrauma* 34, 2941-2949.
11. Phang, I., Zoumprouli, A., Saadoun, S. and Papadopoulos, M.C. (2016). Safety profile and probe placement accuracy of intraspinal pressure monitoring for traumatic spinal cord injury: Injured Spinal Cord Pressure Evaluation study. *J Neurosurg Spine* 25, 398-405.
12. Phang, I., Zoumprouli, A., Papadopoulos, M.C. and Saadoun, S. (2016). Microdialysis to Optimize Cord Perfusion and Drug Delivery in Spinal Cord Injury. *Ann Neurol* 80, 522-531.
13. Saadoun, S., Chen, S. and Papadopoulos, M.C. (2017). Intraspinal pressure and spinal cord perfusion pressure predict neurological outcome after traumatic spinal cord injury. *Journal of Neurology, Neurosurgery & Psychiatry* 88, 452-453.
14. Lacasa, L., Luque, B., Ballesteros, F., Luque, J. and Nuno, J.C. (2008). From time series to complex networks: the visibility graph. *Proc Natl Acad Sci U S A* 105, 4972-4975.
15. Pavlopoulos, G.A., Secrier, M., Moschopoulos, C.N., Soldatos, T.G., Kossida, S., Aerts, J., Schneider, R. and Bagos, P.G. (2011). Using graph theory to analyze biological networks. *BioData Min* 4, 10.

16. Chen, S., Phang, I., Zoumprouli, A., Papadopoulos, M.C. and Saadoun, S. (2016). Metabolic profile of injured human spinal cord determined using surface microdialysis. *J Neurochem* 139, 700-705.
17. Phang, I., Werndle, M.C., Saadoun, S., Varsos, G., Czosnyka, M., Zoumprouli, A. and Papadopoulos, M.C. (2015). Expansion duroplasty improves intraspinal pressure, spinal cord perfusion pressure, and vascular pressure reactivity index in patients with traumatic spinal cord injury: injured spinal cord pressure evaluation study. *J Neurotrauma* 32, 865-874.
18. Newman, M.E. (2006). Modularity and community structure in networks. *Proc Natl Acad Sci U S A* 103, 8577-8582.
19. Watts, D.J. and Strogatz, S.H. (1998). Collective dynamics of 'small-world' networks. *Nature* 393, 440-442.
20. Chen, S., Gallagher, M.J., Papadopoulos, M.C. and Saadoun, S. (2018). Non-linear dynamical analysis of intraspinal pressure signal predicts outcome after spinal cord injury. Submitted.
21. Chesnut, R., Videtta, W., Vespa, P., Le Roux, P. and Participants in the International Multidisciplinary Consensus Conference on Multimodality, M. (2014). Intracranial pressure monitoring: fundamental considerations and rationale for monitoring. *Neurocrit Care* 21 Suppl 2, S64-84.
22. Czosnyka, M., Pickard, J.D. and Steiner, L.A. (2017). Principles of intracranial pressure monitoring and treatment. *Handb Clin Neurol* 140, 67-89.
23. Chesnut, R.M., Temkin, N., Carney, N., Dikmen, S., Rondina, C., Videtta, W., Petroni, G., Lujan, S., Pridgeon, J., Barber, J., Machamer, J., Chaddock, K., Celix, J.M., Cherner, M.,

Hendrix, T. and Global Neurotrauma Research, G. (2012). A trial of intracranial-pressure monitoring in traumatic brain injury. *N Engl J Med* 367, 2471-2481.

24. Adams, H., Donnelly, J., Czosnyka, M., Koliass, A.G., Helmy, A., Menon, D.K., Smielewski, P. and Hutchinson, P.J. (2017). Temporal profile of intracranial pressure and cerebrovascular reactivity in severe traumatic brain injury and association with fatal outcome: An observational study. *PLoS Med* 14, e1002353.

25. Han, J., Yang, S., Zhang, C., Zhao, M. and Li, A. (2016). Impact of Intracranial Pressure Monitoring on Prognosis of Patients With Severe Traumatic Brain Injury: A PRISMA Systematic Review and Meta-Analysis. *Medicine (Baltimore)* 95, e2827.

26. Aries, M.J., Czosnyka, M., Budohoski, K.P., Steiner, L.A., Lavinio, A., Koliass, A.G., Hutchinson, P.J., Brady, K.M., Menon, D.K., Pickard, J.D. and Smielewski, P. (2012). Continuous determination of optimal cerebral perfusion pressure in traumatic brain injury. *Crit Care Med* 40, 2456-2463.

27. Schmidt, J.M., De Georgia, M. and Participants in the International Multidisciplinary Consensus Conference on Multimodality, M. (2014). Multimodality monitoring: informatics, integration data display and analysis. *Neurocrit Care* 21 Suppl 2, S229-238.

28. Le Roux, P., Menon, D.K., Citerio, G., Vespa, P., Bader, M.K., Brophy, G.M., Diring, M.N., Stocchetti, N., Videtta, W., Armonda, R., Badjatia, N., Boesel, J., Chesnut, R., Chou, S., Claassen, J., Czosnyka, M., De Georgia, M., Figaji, A., Fugate, J., Helbok, R., Horowitz, D., Hutchinson, P., Kumar, M., McNett, M., Miller, C., Naidech, A., Oddo, M., Olson, D., O'Phelan, K., Provencio, J.J., Puppo, C., Riker, R., Robertson, C., Schmidt, M., Taccone, F., Neurocritical Care, S. and European Society of Intensive Care, M. (2014). Consensus summary statement of the International Multidisciplinary Consensus Conference on

Multimodality Monitoring in Neurocritical Care : a statement for healthcare professionals from the Neurocritical Care Society and the European Society of Intensive Care Medicine. *Intensive Care Med* 40, 1189-1209.

29. Li, X. and Dong, Z. (2011). Detection and prediction of the onset of human ventricular fibrillation: an approach based on complex network theory. *Physical Review. E: Statistical, Nonlinear, & Soft Matter Physics* 84, 062901.

30. Ahmadlou, M., Adeli, H. and Adeli, A. (2010). New diagnostic EEG markers of the Alzheimer's disease using visibility graph. *J Neural Transm (Vienna)* 117, 1099-1109.

31. Wang, L., Long, X., Arends, J. and Aarts, R.M. (2017). EEG analysis of seizure patterns using visibility graphs for detection of generalized seizures. *J Neurosci Methods* 290, 85-94.

32. Yan, W. and van Serooskerken, E.v. (2015). Forecasting Financial Extremes: A Network Degree Measure of Super-Exponential Growth. *PLoS One* 10, e0128908.

33. Baggio, R. (2013). Studying complex tourism systems: a novel approach based on networks derived from a time series. XIV April International Academic Conference on Economic and Social Development
Moscow, April 2-5, 2013

34. Amaral, L.A., Scala, A., Barthelemy, M. and Stanley, H.E. (2000). Classes of small-world networks. *Proc Natl Acad Sci U S A* 97, 11149-11152.

35. Lacasa, L., Nuñez, A., Roldán, E., Parrondo, J. and Luque, B. (2012). Time series irreversibility: a visibility graph approach. *Eur Phys J B* 85, 217.

36. Bianchi, F.M., Livi, L., Alippi, C. and Jenssen, R. (2017). Multiplex visibility graphs to investigate recurrent neural network dynamics. *Sci Rep* 7, 44037.

Figure Legends

Fig. 1. Patient monitoring and visibility graph construction. **A.** Examples of arterial blood pressure (ABP) and intraspinal pressure (ISP) signals. **B.** ABP and ISP signal data imported in ICM+ to compute other signals e.g. sPRx. **C.** Stages in constructing a visibility graph (top to bottom): The ISP signal is marked at regular intervals (a – g). Visibility lines (red) are drawn to link nodes in the graph. Finally, the adjacency matrix is constructed with entries ‘1’ if two nodes are connected and ‘0’ if not.

Fig. 2. Graph diameter. Diameter is the shortest path between the two most distant nodes.

A. Representative hourly ISP signals from two patients. **B.** Graphs corresponding to the ISP signals in A. with diameters 6 (green) and 14 (red). **C.** Plots of ISP, SCPP and sPRx *versus* graph diameter for all hours in the 58 patients with best-fit trend lines $R = 0.87$, $P < 0.05$ (ISP); $R = -0.96$, $P < 0.0005$ (SCPP); $R = 0.97$, $P < 0.0005$ (sPRx). Mean +/- standard error.

D. Schematic showing effects of various signal fluctuations on graph diameter. a) Sinusoidal, b) Narrow trough, c) Narrow peak, d) Transient baseline increase, e) Large wide peak, f) Peaks on large wide peak.

Fig. 3. Graph modularity. Modularity measures how a graph is structured and identifies communities/clusters. **A.** Representative hourly ISP signals from two patients. **B.** Graphs corresponding to the ISP signals in A. Graph 1, 5 clusters; Graph 2, 10 clusters. Clusters are assigned different colors. **C.** Plots of ISP, SCPP and sPRx *versus* graph modularity for all hours in the 58 patients with best-fit trend lines $R = 0.90$, $P < 0.01$ (ISP); $R = -0.95$, $P < 0.005$ (SCPP); $R = 0.00$, not significant (sPRx). Mean +/- standard error. **D.** Schematic showing effects of various signal fluctuations on graph modularity. a) Sinusoidal, b) Narrow trough, c)

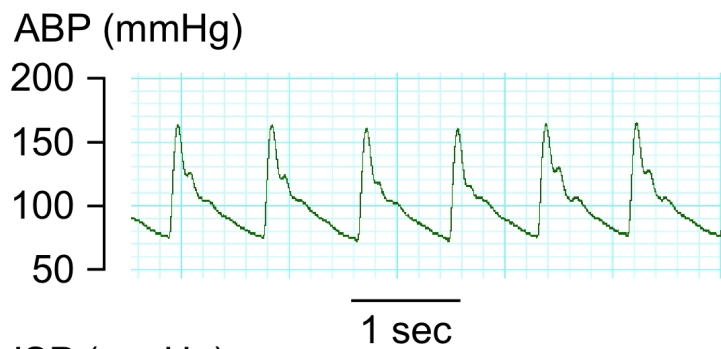
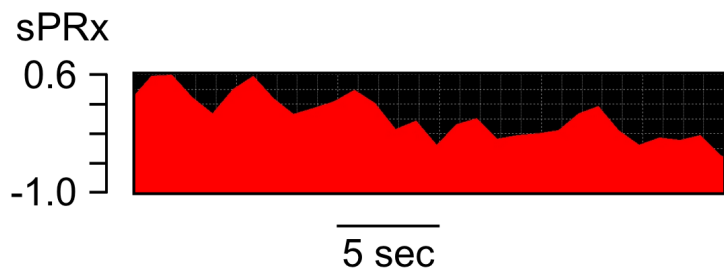
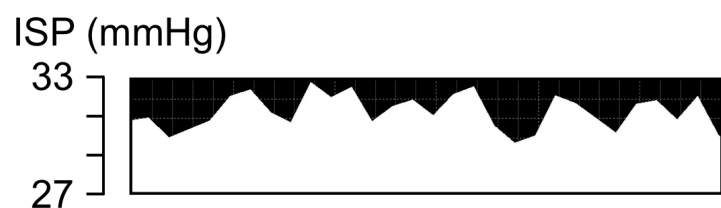
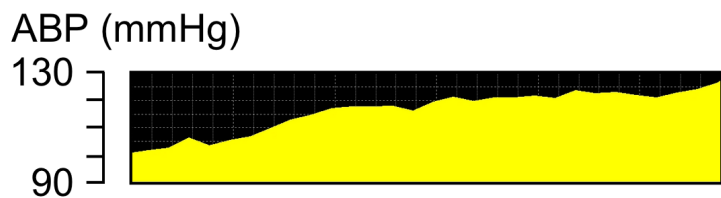
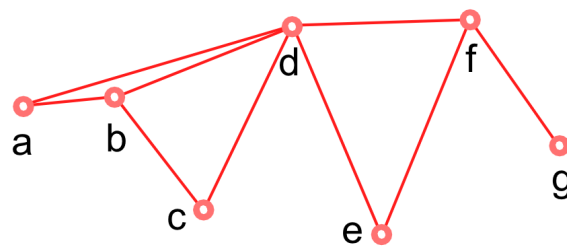
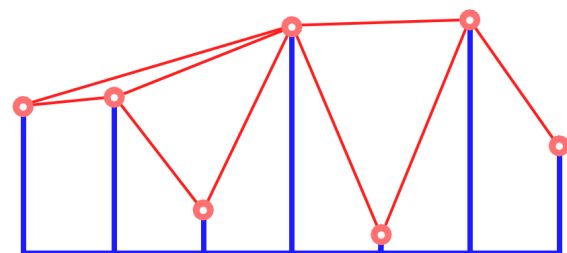
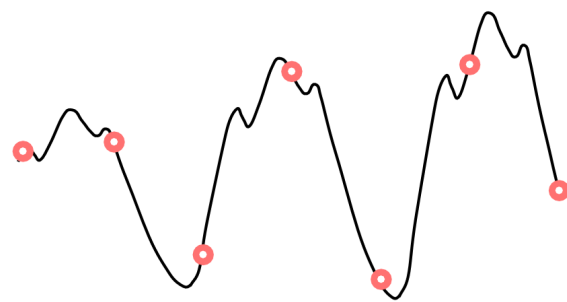
Narrow peak, d) Transient baseline increase, e) Large wide peak, f) Peaks on large wide peak. Two node clusters colored (white, black).

Fig. 4. Graph eccentricity. Eccentricity measures how important nodes are in a graph. **A.** Representative hourly ISP signals from two patients. **B.** Graphs corresponding to the ISP signals in A with nodes colored according to eccentricity. Eccentricity color scale. **C.** Plots of ISP, SCPP and sPRx *versus* graph mean node eccentricity for all hours in the 58 patients with best-fit trend lines $R = 0.87$, $P < 0.05$ (ISP); $R = -0.96$, $P < 0.0005$ (SCPP); $R = 0.98$, $P < 0.0005$ (sPRx). Mean +/- standard error. **D.** Schematic showing effects of various signal fluctuations on eccentricity centrality. a) Sinusoidal, b) Narrow trough, c) Narrow peak, d) Transient baseline increase, e) Large wide peak, f) Peaks on large wide peak. Eccentricity color scale.

Fig. 5. Graph small-worldness. In small-world graphs, most nodes are not directly linked, but any nodes directly linked to a node are likely to be linked to each other. Small-world graphs have coefficient $\sigma > 1$. **A.** Representative hourly ISP signals from two patients. **B.** Graphs corresponding to the ISP signals in A showing node hubs, i.e. node radius proportional to node degree. **C.** Plots of ISP, SCPP and sPRx *versus* graph small worldness for all hours in the 58 patients with best-fit trend lines $R = -0.83$, $P < 0.05$ (ISP); $R = 0.97$, $P < 0.0005$ (SCPP); $R = -0.98$, $P < 0.0005$ (sPRx). Mean +/- standard error. **D.** Schematic showing effects of various signal fluctuations on small-worldness (cluster coefficient CC, average path length APL, CC/APL). a) Sinusoidal (CC = 0.70, APL = 4.73, CC/APL = 0.15), b) Narrow trough (CC = 0.76, APL = 4.09, CC/APL = 0.18), c) Narrow peak (CC = 0.73, APL = 3.36, CC/APL = 0.22), d) Transient baseline increase (CC = 0.73, APL = 3.36,

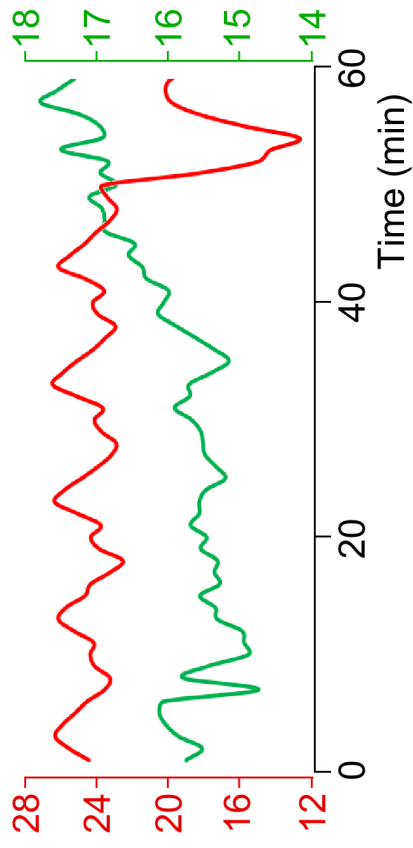
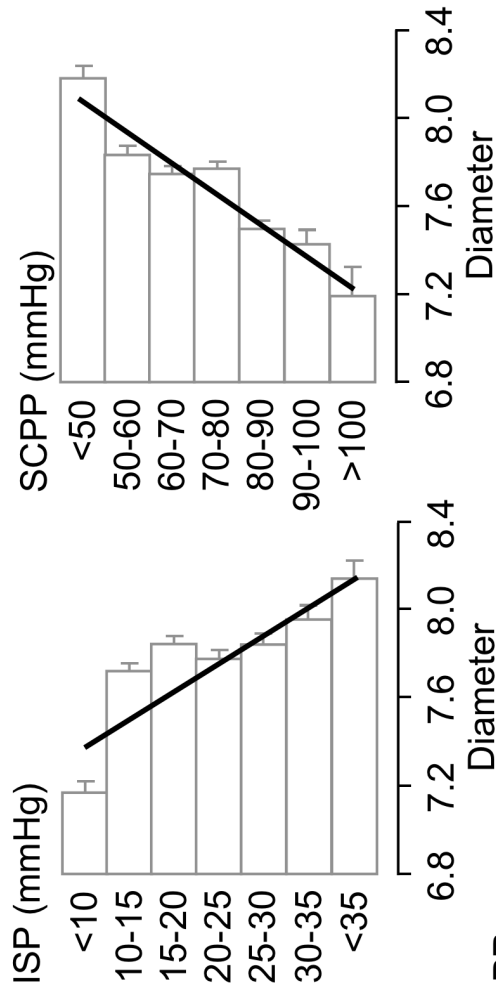
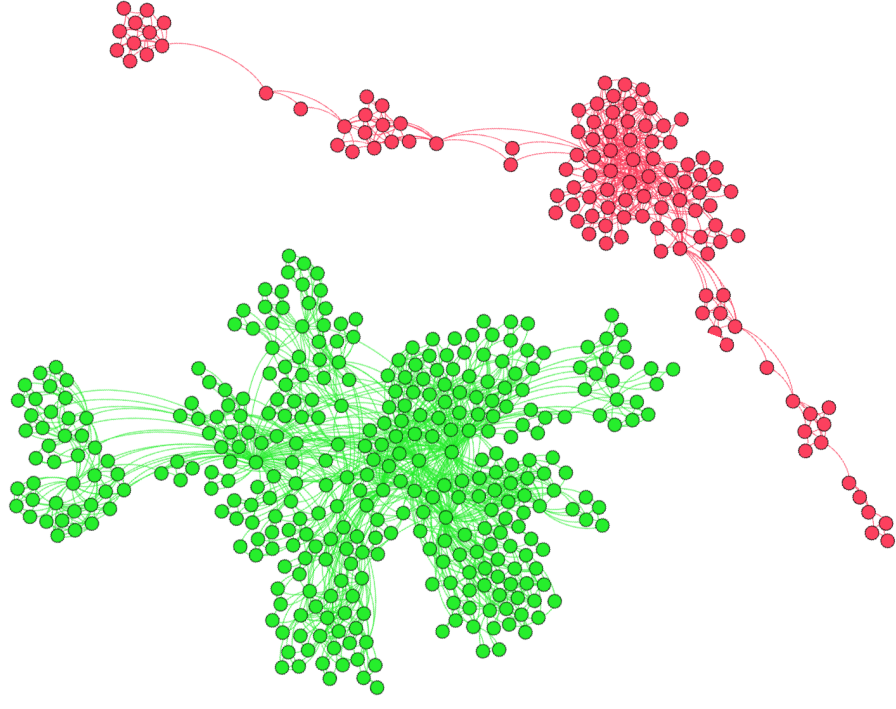
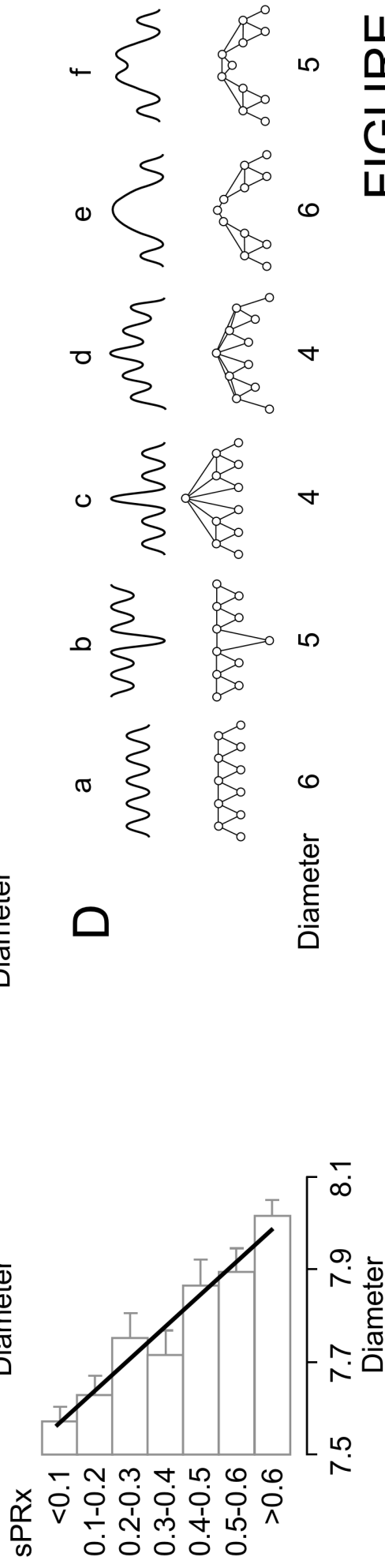
CC/APL = 0.22), e) Large wide peak (CC = 0.61, APL = 5.09, CC/APL = 0.12), f) Peaks on large wide peak (CC = 0.70, APL = 4.09, CC/APL = 0.17).

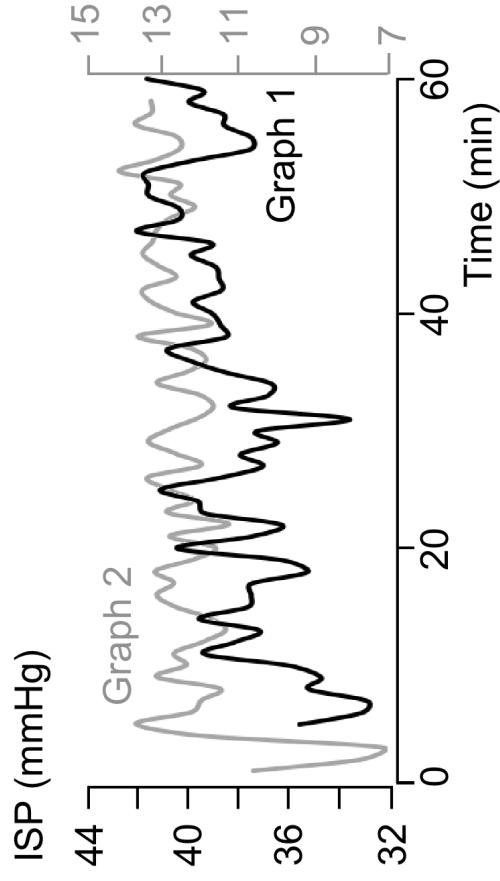
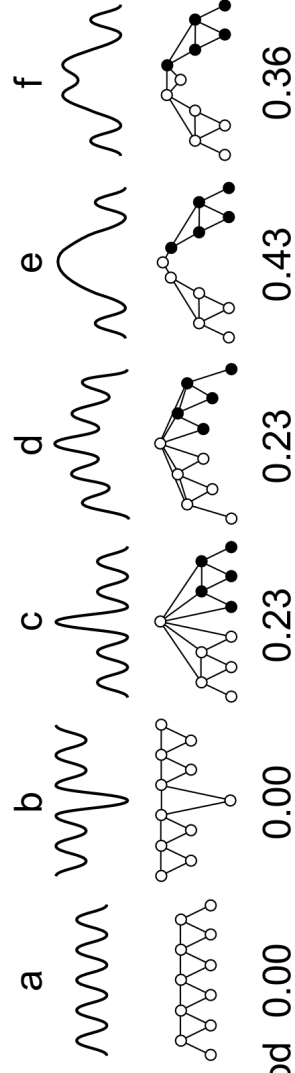
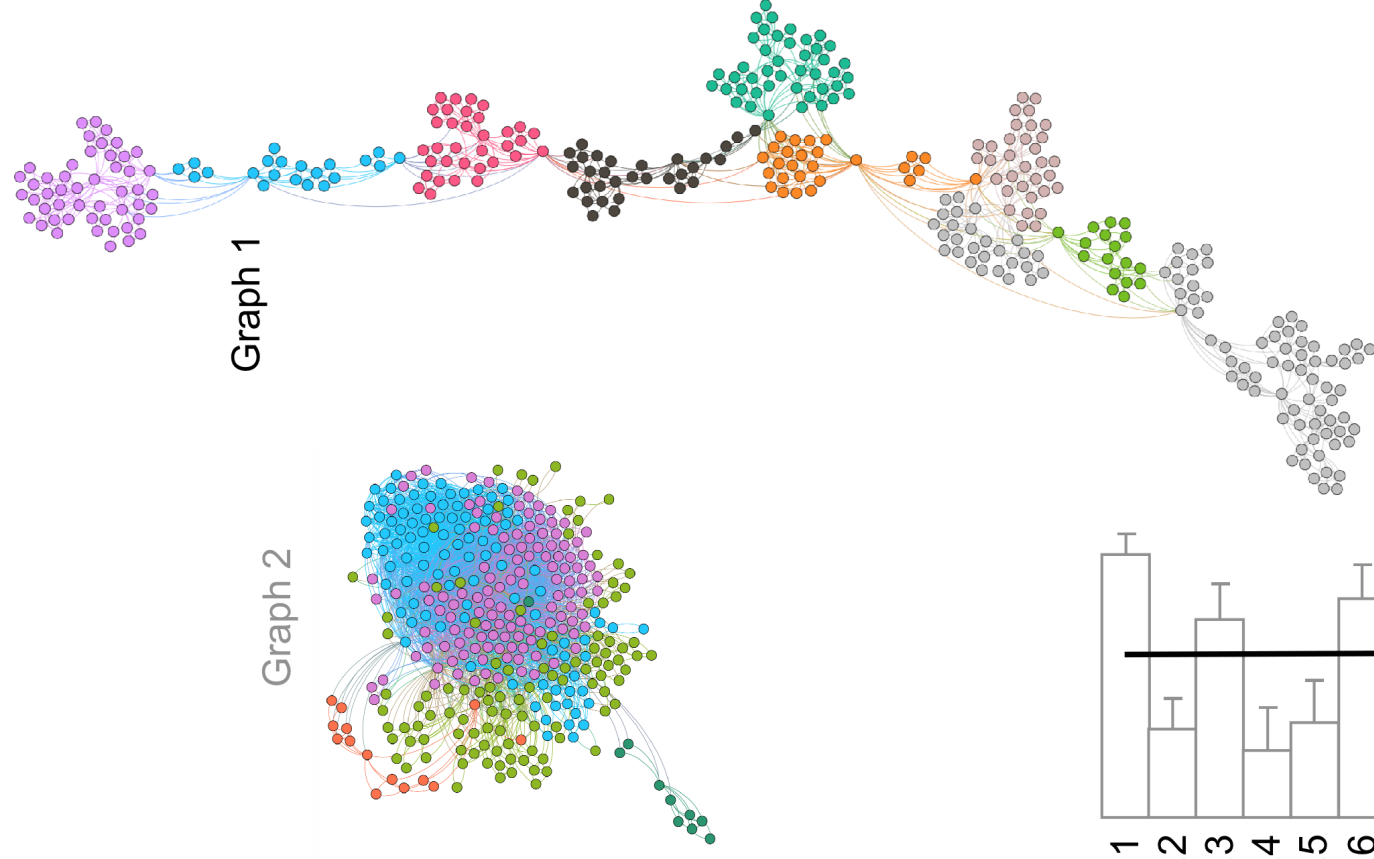
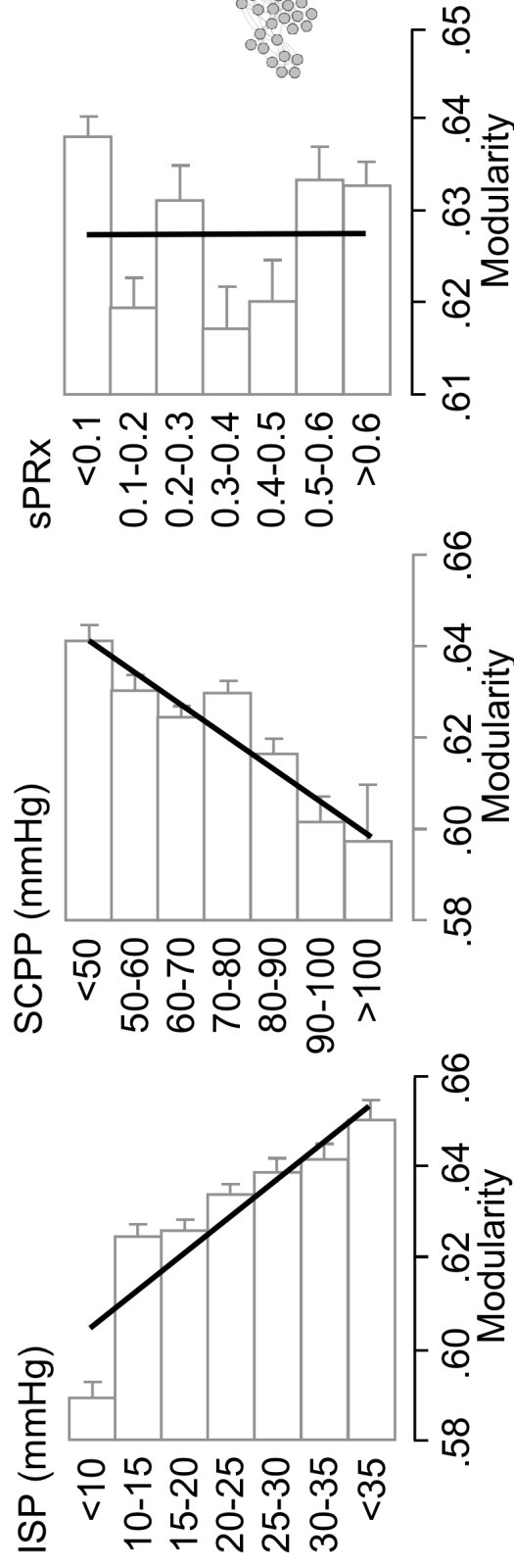
Fig. 6. Neurological outcome. For each patient, we computed average diameter, modularity, mean node eccentricity and small-worldness of all the graphs in the monitoring period. Bar graphs showing **A.** Average patient graph diameter, **B.** Average patient mean node eccentricity, **C.** Average patient modularity, and **D.** Average patient small-worldness *versus* AIS grade change, i.e. AIS grade at follow-up minus AIS grade at presentation. Mean +/- standard error for 57 patients (one of the 58 patients was lost to follow-up).

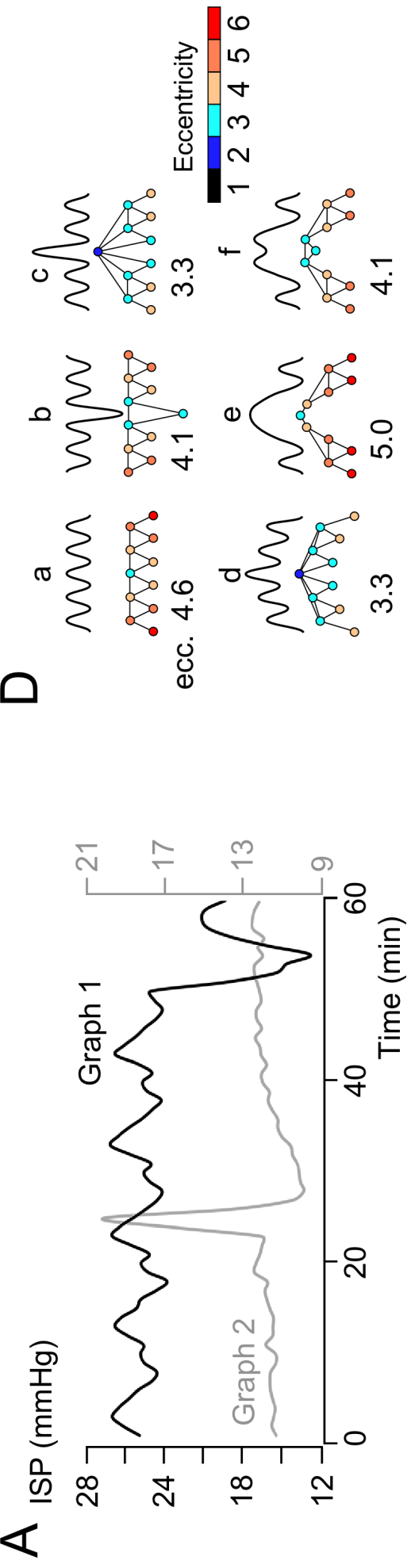
A**B****C**

	a	b	c	d	e	f	g
a	0	1	0	1	0	0	0
b	1	0	1	1	0	0	0
c	0	1	0	1	0	0	0
d	1	1	1	0	1	1	0
e	0	0	0	1	0	1	0
f	0	0	0	1	1	0	1
g	0	0	0	0	0	1	0

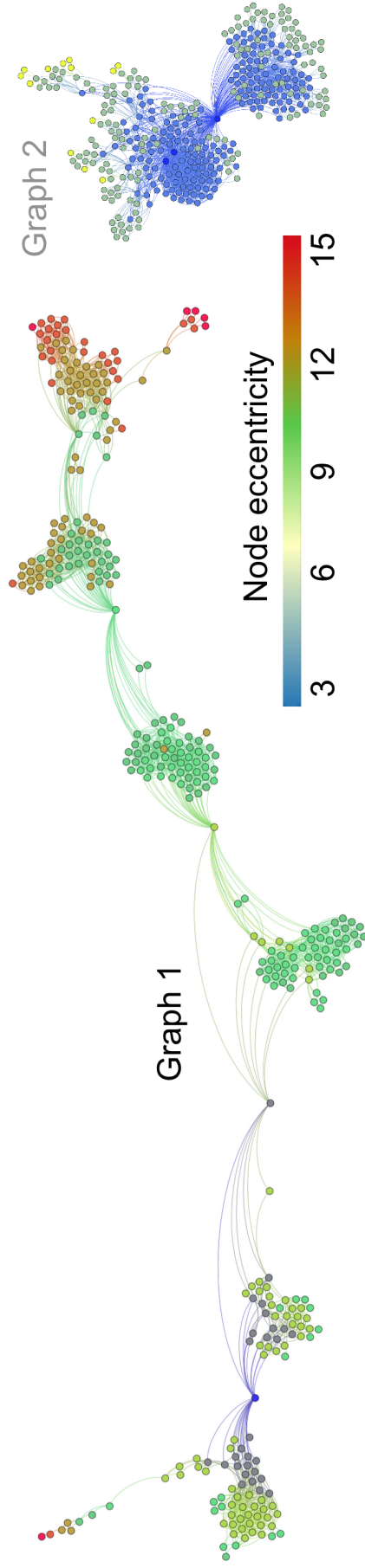
FIGURE 1

A ISP (mmHg)**C****B****D****FIGURE 2**

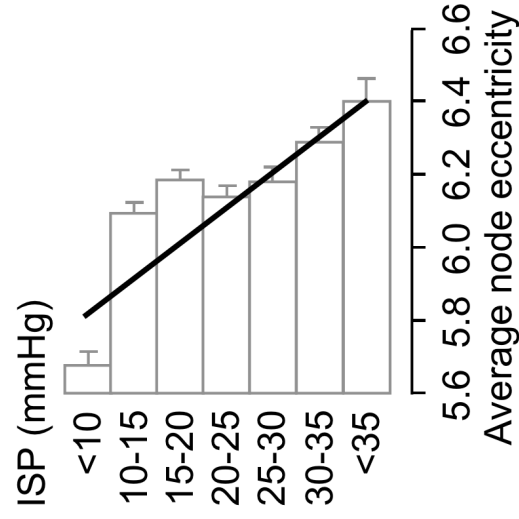
A**D****C**



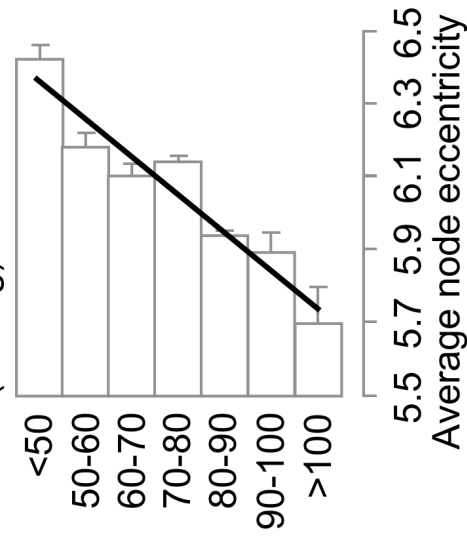
B



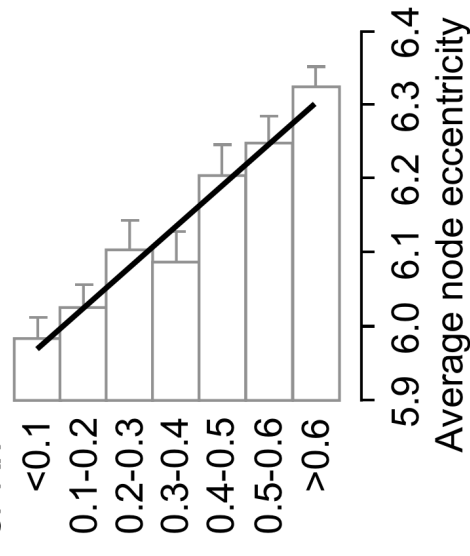
C

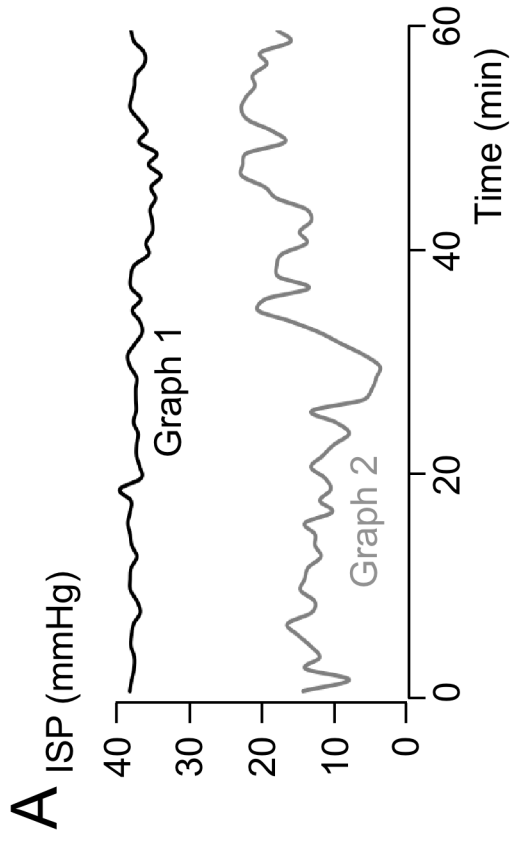


SCPP (mmHg)

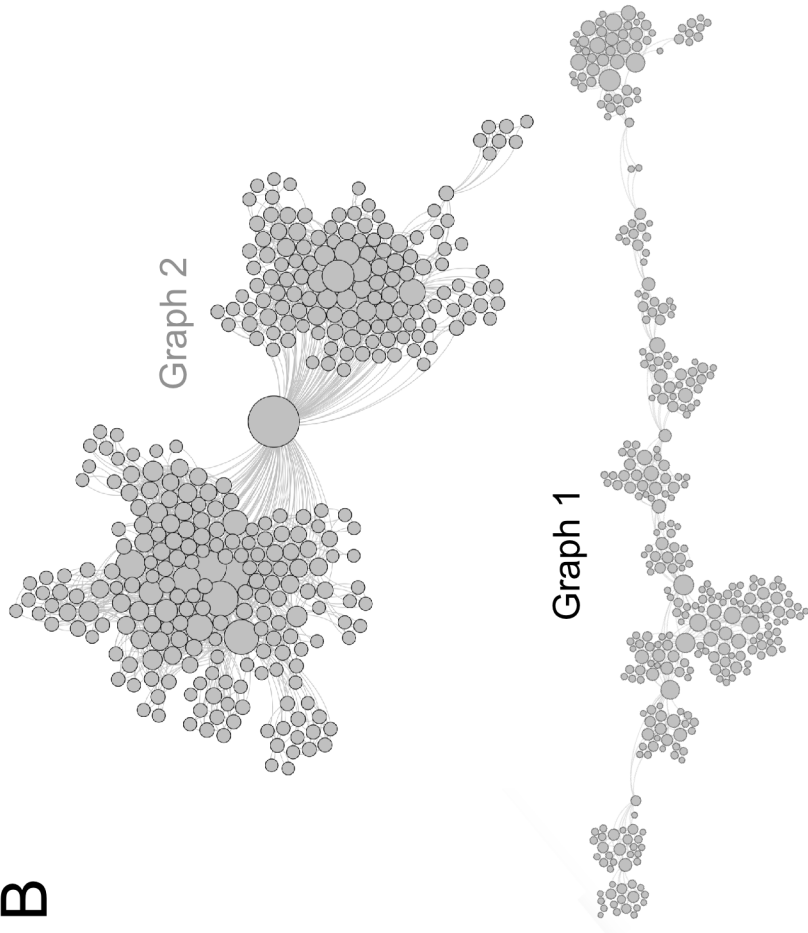


sPRx

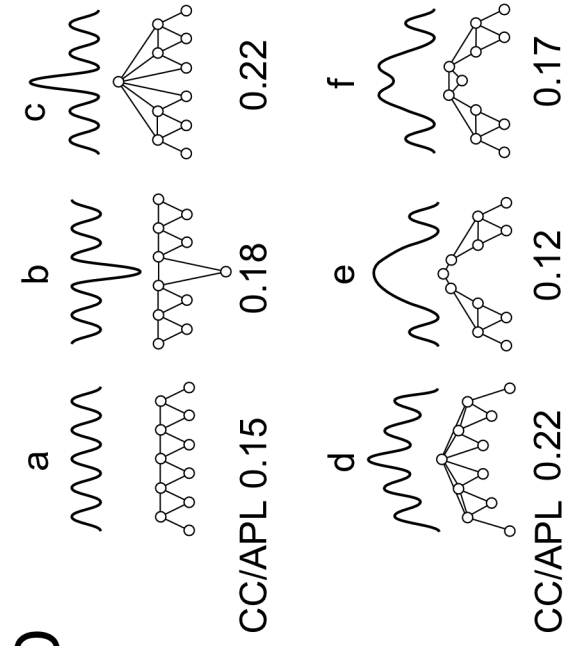




B



D



C

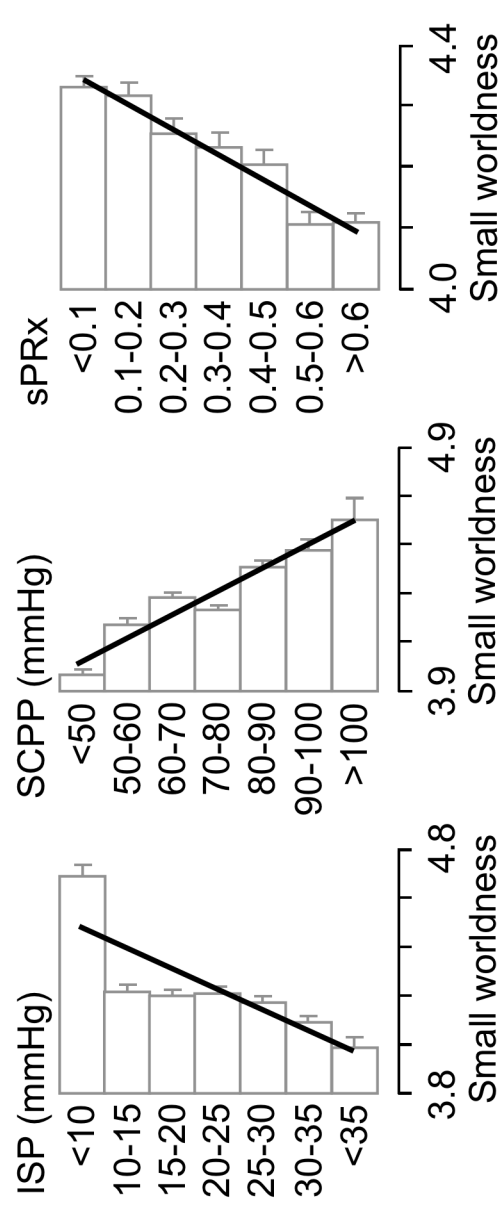


FIGURE 5

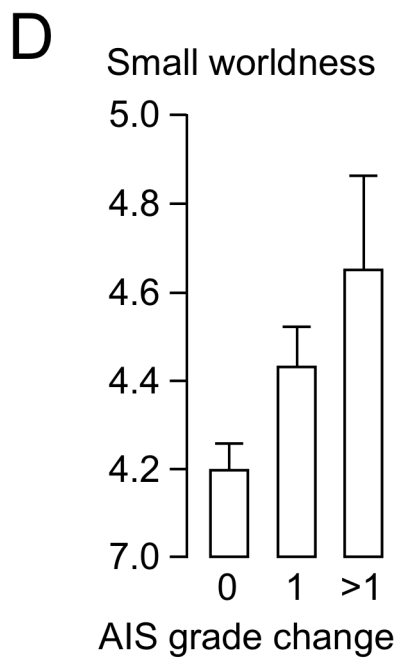
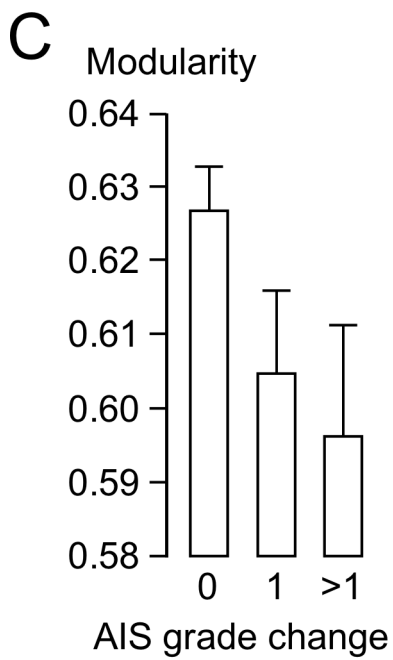
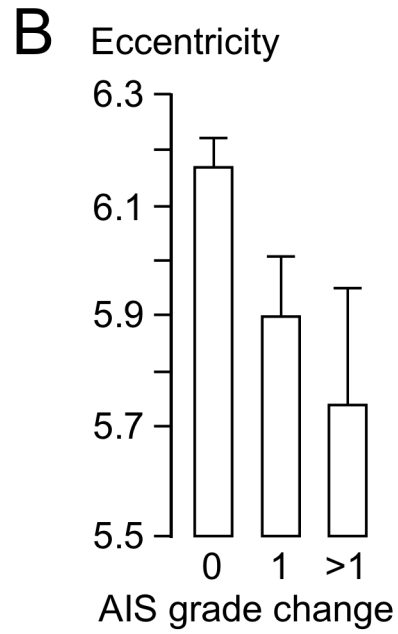
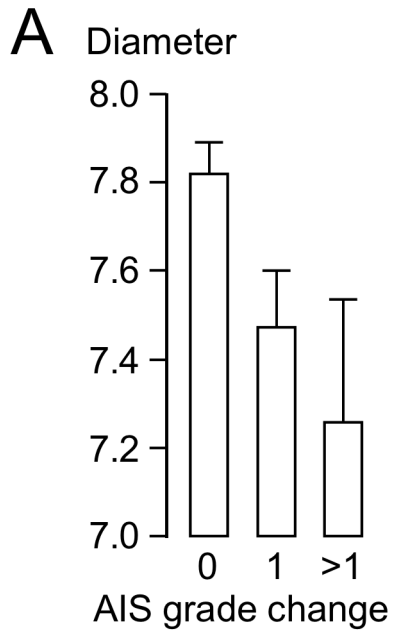


FIGURE 6

Tables 1. Patient demographics.

CHARACTERISTIC	NUMBER
Number of patients	59
Age (mean +/- sem)	41.4 +/- 2.0
Sex (Male : female)	46 : 12
Level of injury (Ce : Th : Lu)	30 : 25 : 3
Surgery (posterior : anterior+posterior)	50 : 8
Admission AIS (A : B : C)	40 : 8 : 10
Follow-up AIS (A : B : C : D : E)	32 : 6 : 7 : 11 : 1
Hours of monitoring (mean +/- sem)	131.4 +/- 4.8
Months of follow-up (mean +/- sem)	18.0 +/- 2.1

AIS, American spinal injuries association Impairment Scale; Ce, cervical; sem, standard error of the mean; Lu, lumbar; Th, thoracic

Table 2. Results of univariate and multivariate logistic regression analysis. Binary outcome was no AIS grade increase (0) *versus* at least 1 AIS grade increase (1).

VARIABLE	UNIVARIATE		MULTIVARIATE	
	OR	P-VALUE	OR	P-VALUE
Admission AIS grade	4.2	<0.001	4.2	<0.05
Patient age (years)	0.9	<0.005		NS
SCPP (mmHg)	1.1	<0.05	1.1	<0.05
ISP (mmHg)	0.9	<0.05		NS
Graph diameter	0.1	<0.005		NS
Graph modularity	0.0	<0.05		NS
Graph eccentricity	0.1	<0.005	0.1	<0.05
Graph small-worldness	14.4	<0.005		NS

AIS, American spinal injuries association Impairment Scale; ISP, intraspinal pressure; NS, not significant; SCPP, spinal cord perfusion pressure

SUPPLEMENT

METHODS

Converting intraspinal pressure signals into graphs. Let $x(t_i)$, $i = 1, 2, 3 \dots$ be an hourly ISP time series window of 360 points (nodes). Nodes i and j ‘see’ each other, thus becoming linked nodes, if all time-series data $(t_k, x(t_k))$ between i and j (i.e. $t_i < t_k < t_j$) meet the requirement:

$$x(t_k) < x(t_i) + [x(t_j) - x(t_i)][(t_k - t_i)/(t_j - t_i)] \quad (\text{Equation 1})$$

This means that nodes i and j can be connected by a straight line such that all nodes between them k where $t_i < t_k < t_j$, lie below this line. Graphs created using the natural visibility algorithm are described by the adjacency matrix A . $A_{ij} = 1$ or 0 depending on whether nodes i and j are linked or unlinked. These graphs are undirected, i.e. $A_{ij} = A_{ji}$.

Graph metrics.

a) *Graph diameter (D)*. The shortest (also called geodesic) path between the two most distant nodes¹⁵:

$$D = \max (d_{ij}) \quad (\text{Equation 2})$$

where d_{ij} is the geodesic distance between nodes i and j . D is the linear size of the graph.

b) *Graph modularity (Q)*. Q measures how a graph is structured and identifies communities/clusters¹⁸. Q is an indicator of graph division – the higher the Q , the stronger the division. Nodes that are grouped together have similar properties and graphs with high Q have dense node links within modules. For n nodes, m links and two clusters let $s_i = 1$ if the node i is in cluster 1 and $s_i = -1$ if in cluster 2. Q is the fraction of links in group 1 or 2 minus the expected number of links in groups 1 and 2 of a random graph with the same node degree distribution:

$$Q = 1/(4m) \sum \{A_{ij} - [(k_i k_j)/2m]\}(s_i s_j + 1) \quad (\text{Equation 3})$$

where \sum is the sum over all node pairs, A_{ij} is the number of links between nodes i and j , $k_i k_j / 2m$ is the expected number of links between nodes i and j (if links were drawn randomly) and k_i, k_j are the degrees of nodes.

- c) *Graph eccentricity (E)*. E is a centrality measure that captures how important nodes are in a graph¹⁵. The E of a node i , $E(i)$, is the geodesic distance, d_{ij} , to its most distant node. A node is more eccentric if it is further away from its most distant node.

$$E(i) = \max (d_{ij}). \quad (\text{Equation 4})$$

where j is any node. We calculated the average E of all nodes.

- d) *Small-worldness*. We first define the average clustering coefficient (CC) of a graph. The CC of node i , c_i , is a number between 0 and 1 that quantifies node link density as:

$$c_i = 2e_i / [k_i(k_i-1)] \quad (\text{Equation 5})$$

where k_i is the number of nodes linked to i (i.e. its neighbors) and e_i is the number of linked pairs between all neighbors of i . CC is the average c_i for all nodes:

$$CC = (1/n) \sum c_i \quad (\text{Equation 6})$$

CC indicates the extent to which neighbors of a node are neighbors of each other. To compute the average path length (APL) we determine the geodesic distances between each pair of nodes, add them up, then divide by the total number of pairs. APL shows, on average, the number of steps it takes to get from one node to another:

$$APL = 1/[n(n-1)] \sum d_{ij} \quad (\text{Equation 7})$$

where d_{ij} is the geodesic distance between nodes i and j . A small-world network, as defined by Watts and Strogatz, is characterized by high CC and short APL¹⁹. Small-worldness is quantified by the coefficient σ , which is calculated by comparing the CC and APL of a graph to an equivalent random graph with same average degree.

$$\sigma = (CC/CC_{\text{random}})/(APL/APL_{\text{random}}) \quad (\text{Equation 8})$$

If $\sigma > 1$, then the graph is small-world.

MULTIVARIATE LOGISTIC REGRESSION ANALYSIS OF AIS GRADE CONVERSION FOR 57 PATIENTS

We used the following settings in the XLSTAT dialogue box:

Model: Logit

Response type: Binary (1 AIS improvement, 0 AIS no improvement)

Confidence interval (%): 95

Model selection: Best model / Likelihood ratio

Min variables: 1 / Max variables: 8

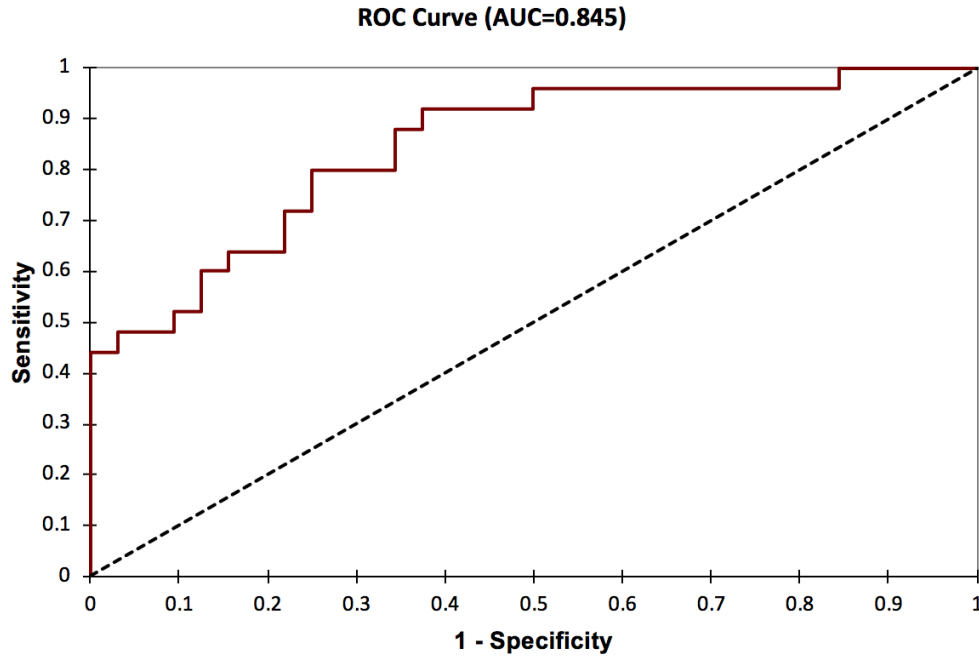
Stop conditions: Iterations = 100 / Convergence = 1E-06

Maximization of the likelihood function using the Newton-Raphson algorithm

The multivariate model parameters were (highlighted):

Source	Value	St. error	Pr > Chi ²	OR	OR LB (95%)	OR UB (95%)
Intercept	11.2	88.4	0.90			
AIS original (A)	1.4	0.5	0.01	4.2	1.5	11.9
Age	0.0	0.0				
Modularity	0.0	0.0				
Diameter	0.0	0.0				
Average of node						
Eccentricity (E)	-2.6	1.2	0.03	0.1	0.0	0.7
Network small worldness	0.0	0.0				
Average of SCPP (SCPP)	0.1	0.0	0.04	1.1	1.0	1.1
Average of ISP	0.0	0.0				

Equation of model: $\text{Pred}(\text{At least 1 AIS increase}) = 1 / (1 + \exp(-(\mathbf{11.235 + 1.432 * A - 2.583 * E + 0.052 * SCPP})))$



ROC curve of the multivariate model of 57 SCI patients. Sensitivity (True Positive Rate = True Positive / (True Positive + False Negative)). Specificity (True Negative Rate = True Negative / (True Negative + False Positive) the area under the curve. Area Under Curve (AUC) quantifies the ability of the model to discriminate between AIS grade improvement (1) and no improvement (0). In a perfect model, AUC = 1. In a random model, AUC = 0.5. In general, AUC between 0.7 and 0.9 indicates a good model and AUC > 0.9 an excellent model.

Classification accuracy assessed by Leave One Out cross validation (LOO-CV).

from \ to	0	1	Total	% correct
0	27	5	32	84.38%
1	10	15	25	60.00%
Total	37	20	57	73.68%

AIS grade increase = 1, No AIS grade change = 0

